COMMUNICATION

Selectivity Boost in Partial Hydrogenation of Acetylene via Atomic Dispersion of Platinum over Ceria

Olumide Bolarinwa Ayodele,*[a] Simone Vinati,[b,†] Emanuele Barborini,[b,‡] Loukya Boddapati,[a] Khalil El Hajraoui,[a] Jutta Kröhnert,[c] Francis Leonard Deepak,[a] Annette Trunschke,[c] Yury V. Kolen'ko*[a]

Received 00th January 20xx,
Accepted 00th January 20xx

DOI: 10.1039/x0xx00000x

A high-throughput flame spray pyrolysis directly affords low-loading Pt catalyst supported on cerium oxide, which is an excellent material for selective semihydrogenation of C_2H_2 at 180 °C, exhibiting nearly complete conversion of C_2H_2 (98.2%) with high selectivity towards C_2H_4 (87.1%). Pt in this catalyst is atomically dispersed within cerium oxide, and this structural feature restricts C_2H_4 adsorption as **π**-bonded, known to promote C_2H_4 selectivity.

Partial hydrogenation of C_2H_2 is an important industrial process for converting traces of C_2H_2 in the C_2H_4 product stream from naphtha cracker to C_2H_4 ($C_2H_2 + H_2 \rightarrow C_2H_4$), otherwise C_2H_2 will poison the Ziegler–Natta catalyst during olefin polymerization. An industrial catalyst for this reaction is $PdAg/Al_2O_3$ with typical Pd weight loadings of 0.03%,[1] which unfortunately deactivates with time due to the formation of subsurface H in the form of β-PdH hydride and coke build-up on active Pd sites.[2] Using smaller Pd clusters and bimetallic systems provides a useful strategy for overcoming these drawbacks. Small Pd sizes shift the metal *d*-band center downward relative to the Fermi level (E_F), which weakens the adsorption of C_2H_4, and thus facilitates C_2H_4 turnover preventing undesired subsequent hydrogenation of C_2H_4 to C_2H_6.[3] Alloying of Pd with metals, such as Ag, Ga, Au, Cu, Zn, renders the active Pd sites spatially isolated, which prevents coking while increasing the selectivity towards C_2H_4 via a site-isolation concept.[4] Reducing catalyst acidity is another approach to tackle its deactivation (fouling), resulting from the formation of green oil and carbonaceous deposits.

Recently, we embarked on the investigation of catalysts for partial hydrogenation of C_2H_2. Initially, we were interested in understanding the behavior of Pd catalysts using combined experimental–theoretical approach.[5] The catalyst achieved a high C_2H_2 conversion $X_{C2H2} \approx 97\%$ but a rather poor selectivity towards C_2H_4 $S_{C2H4} \approx 62\%$. Importantly, there was a qualitative and quantitative match between experimental results and computational modeling. Further, motivated by the reduction of the catalyst's cost while improving its selectivity, we theoretically explored and experimentally realized bimetallic PtCu,[6] showing high selectivity $S_{C2H4} \approx 85\%$ at near-complete X_{C2H2}. In the present study, we turn our attention to continuously expanding the concept of atomically dispersed catalysts, which show high activity and selectivity owing to the enhanced density and low coordination number of active sites homogeneously distributed through the supporting material.[7] Herein, we disclose a general approach for scalable preparation of Pt catalyst atomically dispersed over CeO_2 support through a high-throughput flame spray pyrolysis (FSP) method.

Notably, the FSP aerosol synthesis of nanostructured materials is a well-established method for the gas-phase production of a wide variety of nanoparticles.[8] In the FSP, a liquid solution containing the correct stoichiometry of elements of interest (typically in the form of organometallics or nitrates) is sprayed into a flame. Here, the chemicals are pyrolyzed and the contained elements are released in the gas phase to form nanoparticles composed by the same elements. One of the main advantages of FSP is the single-step synthesis of complex nanoparticles without the necessity of post-treatments, such as calcination.[9] Moreover, in the last decades, FSP was scaled-up to industrial exploitation, becoming a competitive alternative to traditional nanoparticle preparation methods, economically as well as from the environmental point of view.[10, 11]

We intended to develop a highly dispersed Pt/CeO_2 catalyst as well as cluster Pt/CeO_2 catalyst and compare their ability to accomplish selective hydrogenation of C_2H_2 to C_2H_4. For this purpose, two catalysts with low 0.23%Pt/CeO_2 and high 5%Pt/CeO_2 platinum loadings were synthesized by FSP, along with pure CeO_2 and 0.5%Pt/CeO_2 for comparison (Fig. S1). A detailed description of synthesis, characterization, and catalytic testing are presented in the ESI. The physicochemical properties

---

[a] *International Iberian Nanotechnology Laboratory, Braga 4715-330, Portugal. E-mail: oluayodele@outlook.com, yury.kolenko@inl.int*
[b] *Tethis S.p.A., Milan 20143, Italy.*
[c] *Department of Inorganic Chemistry, Fritz-Haber-Institut der Max-Planck-Gesellschaft, Berlin 14195, Germany.*
† Present address: ParteQ GmbH, Malsch 76316, Germany.
‡ Present address: Luxembourg Institute of Science and Technology, Esch-sur-Alzette 4362, Luxembourg.

Electronic Supplementary Information (ESI) available. See DOI: 10.1039/x0xx00000x

of the catalysts were systematically studied and correlated with the performance in partial hydrogenation of C_2H_2.

We began by studying the catalytic properties of the as-synthesized catalysts. It is well known that FSP results in the formation of oxide products due to the oxidative burning principle of the technique, and accordingly, the Pt phase is expected to appear as PtO in the resultant catalysts (Fig. S2).[12] Hence, for catalytic testing, the materials were first subjected to reduction in H_2/He mixture at the respective temperatures established by H_2 temperature-programmed reduction (H_2–TPR). To eliminate the possible effect of particle size variation, the temperature (*T*) was brought to the highest reaction temperature (R_XT) of catalytic testing, and the reaction products were measured as the *T* ramped down at a programmed rate.

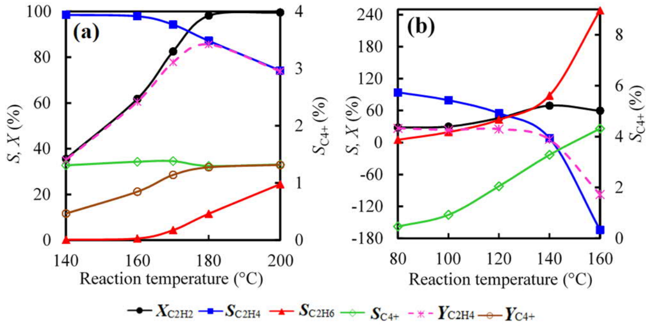

Fig. 1 Catalytic properties of 0.23%Pt/CeO_2 (a) and 5%Pt/CeO_2 (b) catalysts as a function of reaction temperature R_XT. Space velocity of 630 000 mL g^{-1} h^{-1}.

The reactor feed composition was close to industrial settings, simulating the gas mixture having the excess of C_2H_4 in the stream under atmospheric pressure, viz, 1, 20, 20, 59 mL min^{-1} of C_2H_2, C_2H_4, H_2, He, respectively. Figs. 1a,b show conversion (*X*) of C_2H_2, selectivity (*S*) towards C_2H_4, C_2H_6, and combined but-1-ene plus buta-1,3-diene (C4+) products and their yields (*Y*) as a function of R_XT. Exploration of catalytic properties of 0.23%Pt/CeO_2 revealed that X_{C2H2} increases with R_XT, while S_{C2H4} reduces, and S_{C2H6} increases at high R_XT. This is consistent with thermodynamic consideration, wherein full hydrogenation to C_2H_6 is favored at higher temperatures ($C_2H_2 + H_2 \rightarrow C_2H_4$, $\Delta H° = -175.4$ kJ mol^{-1}; $C_2H_4 + H_2 \rightarrow C_2H_6$, $\Delta H = -136.9$ kJ mol^{-1}). The best results for 0.23%Pt/CeO_2 were obtained at 180 °C, where the catalyst achieves $X_{C2H2} = 98.2\%$ with excellent $S_{C2H4} = 87.1\%$. Further increase of R_XT to industrially-relevant 200 °C leads to enhanced $X_{C2H2} = 99.6\%$ albeit with ≈13% loss in $S_{C2H4} = 74.2\%$, leading to an increase in S_{C2H6} and Y_{C4+} (Fig. 1a).

On the other hand, the 5%Pt/CeO_2 catalyst shows a deviating trend in performance (Fig. 1b). As R_XT increases, the X_{C2H2} also increases and reaches a maximum at 140 °C with $X_{C2H2} = 70\%$. At 140 °C, S_{C2H4}, however, drastically reduces to 8.3%, while S_{C2H6} and S_{C4+} increase to 88.4% and 3.3%, respectively. As the *RxT* increases further to 160 °C, X_{C2H2} reduces to 59.6%, while S_{C2H4} dived to –163.7%, and both S_{C2H6} and S_{C4+} increased to 248.1% and 4.3%, respectively. The negative S_{C2H4} and $S_{C2H6} > 100\%$ imply that both C_2H_2 and substantive amounts of co-fed C_2H_4 underwent full hydrogenation to C_2H_6. Notably, in the absence of Pt, pure CeO_2 was found to be inactive for C_2H_2 hydrogenation in all R_XT tested (80–200°C).

The above catalytic results unambiguously demonstrate that our newly developed 0.23%Pt/CeO_2 significantly outperforms 5%Pt/CeO_2 in terms of desired C_2H_4 product yield, providing maximum $Y_{C2H4} = 85.5\%$ at 180 °C with stable activity and selectivity after the time-on-stream (TOS) testing for at least 10 h (Fig. S3). Moreover, this high-performing catalyst contains >20 times less amount of Pt, which also plays a positive role in the development of cost-effective catalytic materials. Similarly, when compared with some selected state-of-the-art catalysts, including the industrial PdAg catalyst, 0.23%Pt/CeO_2 obviously outperformed them, especially when the amount of active metal loading, R_XT, and space velocity is considered (Table S1).[4, 6, 13-20] Therefore, we were interested in understanding the reasons behind the excellent activity and selectivity of 0.23%Pt/CeO_2 as compared to 5%Pt/CeO_2.

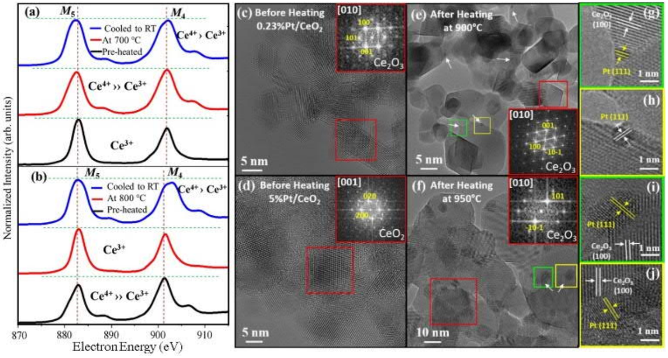

Fig. 2 EELS spectra of Ce–$M_{4,5}$ edges for 0.23%Pt/CeO_2 (a) and 5%Pt/CeO_2 (b) acquired at different experimental conditions: before, during, and after heat treatment, as indicated in the legends. The oxidation states are predicted from Ce–$M_{4,5}$ line ratios, as well as from the spectral shapes. (c) and (d) are HRTEM images and the corresponding Fast Fourier Transforms (FFTs) for 0.23%Pt/CeO_2 and 5%Pt/CeO_2 sample before heating, while (e) and (f) are their respective HRTEM images and FFTs after heating. (g) and (h) are the zoom-in images of Pt nanoclusters (marked with white arrows in (e)) appearing after heating. (i) and (j) are the zoom-in images of a Pt nanocluster (marked with a white arrow in (f)) appearing after heating.

To this end, we employed *in situ* non-isothermal electron energy-loss spectroscopy (EELS), which can simultaneously investigate both electronic and structural properties. The M_5/M_4 intensity ratios, the spectral features, and broadening parameters have been identified to be sensitive to the chemical state of Ce, and the oxidation state can be determined such that $M_5 > M_4$ indicates Ce^{3+} oxidation state and *vice versa*.[21] According to the EELS analysis, the predominant Ce oxidation states were found to be 3+ and 4+ in 0.23%Pt/CeO_2 and 5%Pt/CeO_2, respectively (Figs. 2a,b). This result was further corroborated by high-resolution transition electron microscopy (HRTEM), which confirms the presence of Ce_2O_3 in 0.23%Pt/CeO_2 and CeO_2 in 5%Pt/CeO_2 (Figs. 2c,d). These results showed that the low Pt loading caused obvious defects in the support structure leading to higher concentrations of Ce^{3+} and a large number of O vacancies.

Interestingly, in our intensive studies of 0.23%Pt/CeO_2 by HRTEM, high-angle annular dark-field scanning transmission electron microscopy (HAADF–STEM), and energy-dispersive X-ray spectroscopy (STEM–EDX), no evidence of Pt being present in the as-synthesized catalyst was found (Figs. 2c, 3a). We

This journal is © The Royal Society of Chemistry 20xx

hypothesized that if Pt exists in the sample, as suggested by catalytic results, they would appear at high temperatures due to segregation. Hence, we subjected 0.23%Pt/CeO_2 to *in situ* TEM heating experiment (to 900 °C, Video S1), and in fact, the experiment shows the evolution of Pt at 900 °C (Figs. 2e, 3b). The following electron microscopy analysis of the heated 0.23%Pt/CeO_2 confirms the formation of small 1–2 nm Pt clusters as a result of Pt segregation at $T \geq 800$°C (Figs. 2e,g,h, 3b). We also conducted similar experiments for the catalyst with 5% Pt loading. Unlike 0.23%Pt/CeO_2, the scarce presence of small Pt clusters was already observed in the as-synthesized 5%Pt/CeO_2 (Fig. 3c). Moreover, the *in situ* TEM heating analysis of the sample shows a significant growth of the Pt clusters with an increase in temperature, leading to the formation of 3–6 nm clusters after heating to 900 °C (Video S2, Figs. 2f,i,j, 3d).

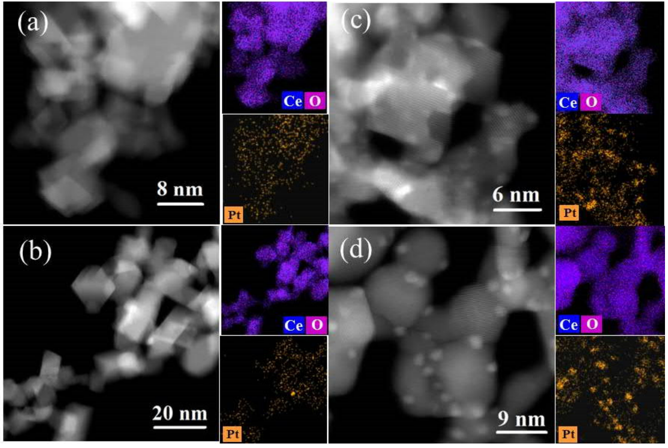

Fig. 3 HAADF–STEM images of 0.23%Pt/CeO_2 (a,b) and 5%Pt/CeO_2 (c,d) catalysts before (a,c) and after (b,d) *in situ* TEM heating experiment to 900 °C, together with the corresponding STEM–EDX elemental maps for Pt and Ce/O mixture.

The variation of the Pt cluster sizes also reflected in the samples' textural properties (Fig. S4, Table S2). The pore structure of the samples showed that the FSP synthesis leads to the formation of mesoporous Ce oxide. Whereas 0.23%Pt/CeO_2 demonstrates no significant variation in textural properties as compared to the pure CeO_2 control, 5%Pt/CeO_2 shows a slight increase in textural properties, most likely due to the contribution from the presence of Pt nanoclusters.

The electron microscopy investigation suggests that there is a unique conceptual difference between 0.23%Pt/CeO_2 and 5%Pt/CeO_2 catalysts where the catalysts with 5% Pt loading is, at least in part, Pt nanoclusters supported on cerium(iv) oxide, i.e. CeO_2. On the other hand, the 0.23% Pt loading most likely leads to the formation of highly dispersed Pt over Ce_2O_3, perhaps in the form of single-atom or a solid solution. Therefore, we investigated whether dispersed and clustered Pt interacts with cerium oxide support differently using H_2–TPR (Fig. 4a). We found that pure CeO_2 control shows two peaks at 486 and 873 °C, which reflect the reduction of the surface (O_S) and bulk (O_B) lattice oxygen.[22] The O_B peak appears unperturbed for all three samples. In contrast, O_S peaks of the Pt catalysts shift towards lower reduction temperatures due to Pt interaction with the oxide support via a somewhat Mars-van Krevelen-like mechanism. While the PtO reduction peak of 5%Pt/CeO_2 is well-separated from its O_S peak, the PtO and O_S peaks of 0.23%Pt/CeO_2 were found to be conjugated, highlighting strong metal–support interaction (SMSI) in the catalyst.[23] Moreover, X-ray photoelectron spectroscopy (XPS) analysis of the catalysts indicates that the binding energy (BE) of Pt 4*f*, usually seen at 72.4 eV, shifted to a lower BE of 72.1 eV in 5%Pt/CeO_2 and a higher BE of 72.6 eV in 0.23%Pt/CeO_2 (Fig. 4b). Although the observed +0.20 eV shift for 0.23%Pt/CeO_2 is rather small and could be affected by other contributions, such as band bending and final state effects, we believe that this shift is a confirmation of SMSI in the catalyst due to combined electronic modulation.[24]

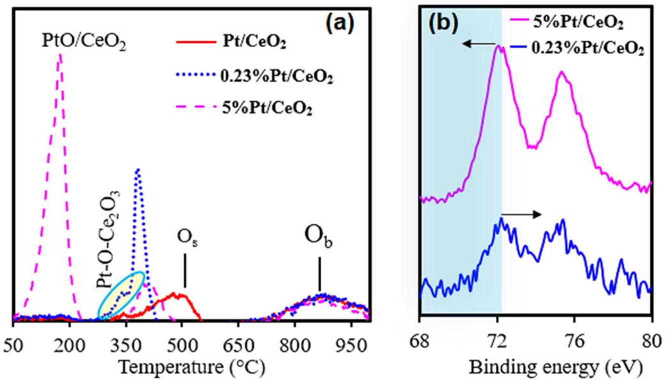

Fig. 4 (a) Comparison of H_2–TPR behavior of control pure CeO_2 support as well as 0.23%Pt/CeO_2 and 5%Pt/CeO_2 catalysts. (b) Comparison of XPS narrow scans of the Pt 4*f* region for 0.23%Pt/CeO_2 and 5%Pt/CeO_2.

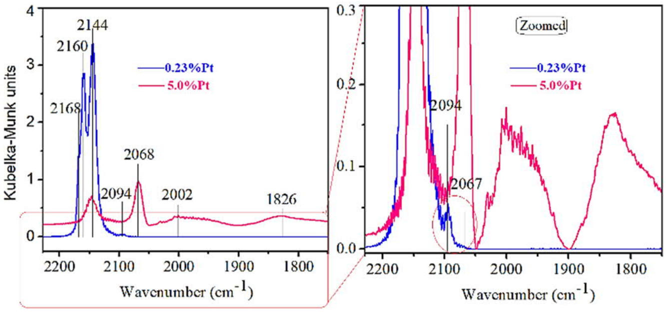

Fig. 5 Comparison of DRIFT spectra of CO adsorption over 0.23%Pt/CeO_2 and 5%Pt/CeO_2 catalysts.

The above results indicate that the high-performing 0.23%Pt/CeO_2 catalyst exhibits dispersed Pt strongly interacting with cerium oxide. Pt in this catalyst is likely to be either confined within cerium oxide or atomically dispersed, influencing the binding of the reactive molecules differently. Therefore, we subjected the catalysts (after reduction in H_2/He) to CO adsorption using diffuse reflectance infrared Fourier transform (DRIFT) spectroscopy, and the results are plotted in Fig. 5. The peaks observed at higher wavenumbers, 2168, 2160, and 2144 cm^{-1}, are ascribed to CO adsorbed on Ce^{n+}, CO in contact with OH groups, and physisorbed CO, respectively.[25] We found that 5%Pt/CeO_2 adsorbed CO at 2068, 1950, and 1837 cm^{-1}, which are due to linear, isolated bridged, and tri-coordinated bonds.[26] This result demonstrates that 5%Pt/CeO_2 is characterized by the presence of Pt in form of clusters with varying sizes, and it is consistent with our electron microscopy study. In sharp contrast, 0.23%Pt/CeO_2 demonstrates only one type of CO adsorption over Pt species at 2094 cm^{-1}, which is associated with the presence of a significant density of atomically dispersed $Pt^{\delta+}$ in the catalyst.[25, 27]

To gain deeper understanding of the CO adsorption over different Pt species, another CeO_2-supported catalyst with 0.5%Pt loading (0.5%Pt/CeO_2) was synthesized and studied. On the one hand, the DRIFT spectroscopy demonstrates that as the Pt loading increased from 0.23% to 0.5%, the resultant 0.5%Pt/CeO_2 catalyst is still characterized by only one type of CO adsorption (Fig. S5). On the other hand, the CO adsorption peak slightly shifts to lower wavenumber of 2067 cm^{-1}, which has been attributed to the presence of Pt sub-nanometre clusters,[28] and not to atomically dispersed Pt.

The catalytic activity study shows that 0.5%Pt/CeO_2 achieves near-complete X_{C2H2} of 98.3% at 180 °C, which is similar to the 0.23%Pt/CeO_2, while the S_{C2H4}, S_{C2H6} and S_{C4+} over 0.5%Pt/CeO_2 appear to be somewhat in-between atomically dispersed 0.23%Pt/CeO_2 and cluster 5%Pt/CeO_2 catalysts (Fig. S6). Moreover, 0.5%Pt/CeO_2 provides the maximum Y_{C2H4} of 55.8% at 150 °C, which is barely 10 °C higher than what was observed over cluster 5%Pt/CeO_2 catalyst (Fig. 1b). This trend suggests that 0.5%Pt/CeO_2 exhibits a significant structural similarity with the 5%Pt/CeO_2 catalyst rather than with atomically dispersed 0.23%Pt/CeO_2 material.

Apparently, there is significant variation in the structural and electronic properties between atomically dispersed and nanocluster Pt catalysts, and this structural specificity of the catalyst governs the observed catalytic performance. Specifically, three modes for C_2H_4 adsorption over catalyst have been reported: π-bonded, di-σ-bonded, and ethylidyne. Ethylidyne species exhibit the highest initial adsorption heat (185 kJ mol^{-1}) resulting from the dissociation adsorption of C_2H_4 on the 3-fold adjacent metal atoms, which easily induces the over-hydrogenation of acetylene to ethane.[29] Based on our results, one can deduce that atomic dispersion of Pt in 0.23%Pt/CeO_2 restricts excessive C_2H_4 adsorption, thus clearly demonstrating the importance of π-bonded configuration in achieving selectivity towards desired C_2H_4 product (Fig. 1a). Importantly, this observation is in good agreement with the previously reported literature on AgPd, AuPd, CuPt bimetallic[6, 30, 31], and Pt single atom[28] catalysts. On the other hand, in 5%Pt/CeO_2 catalyst larger sizes of Pt clusters with varying size distribution is responsible for multi-σ bonding of C_2H_4, thus inducing the undesired increase in the S_{C2H6} and S_{C4+} especially as the temperature increases (Fig. 1b).[32]

In conclusion, high-throughput flame spray pyrolysis is a viable method for the synthesis of either nanocluster or atomically dispersed Pt catalysts supported on cerium oxide. In partial hydrogenation of C_2H_2 to C_2H_4 at 180 °C, the new atomically dispersed 0.23%Pt/CeO_2 catalyst is stable and achieves nearly full conversion of 98.2% delivering high selectivity of 87.1%. Notably, this catalyst significantly outperforms the 5%Pt/CeO_2 nanocluster catalyst that is prone to undesired full hydrogenation of C_2H_2 to C_2H_6. Atomic dispersion of Pt over cerium oxide favors weak π-bonded adsorption of C_2H_4 over the catalyst. In turn, weak bonding facilitates the release of C_2H_4 providing high selectivity towards this product. Overall, we have shown how activity and selectivity of the hydrogenation catalyst can be boosted by atomic dispersion of the active Pt metal while the catalyst cost can be markedly reduced by lowering the mass loading of this rare and expensive element.

Conflicts of interest

There are no conflicts to declare.

Acknowledgments

We thank the members of the Nanochemistry Research Group (http://nanochemgroup.org) at INL for valuable discussions. This work was partially supported by the EU's Horizon 2020 research and innovation program through the CritCat Project under Grant Agreement No. 686053. L.B. acknowledges the EU's Horizon 2020 MSCA COFUND program through the NanoTRAINforGrowth II project.

Notes and references

1. A. N. R. Bos, E. S. Botsma, F. Foeth, H. W. J. Sleyster and K. R. Westerterp, *Chemical Engineering and Processing: Process Intensification*, 1993, 32, 53-63.
2. A. Borodzinski, *Catal Lett*, 1999, 63, 35-42.
3. H. Xin, A. Vojvodic, J. Voss, J. K. Nørskov and F. Abild-Pedersen, *Physical Review B*, 2014, 89, 115114.
4. M. Armbrüster, K. Kovnir, M. Behrens, D. Teschner, Y. Grin and R. Schlögl, *Journal of the American Chemical Society*, 2010, 132, 14745-14747.
5. L. P. L. Gonçalves, J. Wang, S. Vinati, E. Barborini, X.-K. Wei, M. Heggen, M. Franco, J. P. S. Sousa, D. Y. Petrovykh, O. S. G. P. Soares, K. Kovnir, J. Akola and Y. V. Kolen'ko, *International Journal of Hydrogen Energy*, 2020, 45, 1283-1296.
6. O. B. Ayodele, R. Cai, J. Wang, Y. Ziouani, Z. Liang, M. C. Spadaro, K. Kovnir, J. Arbiol, J. Akola, R. E. Palmer and Y. V. Kolen'ko, *ACS Catalysis*, 2020, 10, 451-457.
7. R. T. Hannagan, G. Giannakakis, M. Flytzani-Stephanopoulos and E. C. H. Sykes, *Chemical Reviews*, 2020, DOI: 10.1021/acs.chemrev.0c00078.
8. S. Li, Y. Ren, P. Biswas and S. D. Tse, *Progress in Energy and Combustion Science*, 2016, 55, 1-59.
9. W. Y. Teoh, R. Amal and L. Mädler, *Nanoscale*, 2010, 2, 1324-1347.
10. A. J. Gröhn, S. E. Pratsinis, A. Sánchez-Ferrer, R. Mezzenga and K. Wegner, *Industrial & Engineering Chemistry Research*, 2014, 53, 10734-10742.
11. K. Wegner, B. Schimmoeller, B. Thiebaut, C. Fernandez and T. Rao, *KONA Powder and Particle Journal*, 2011, 29, 251-265.
12. R. Strobel, A. Baiker and S. E. Pratsinis, *Advanced Powder Technology*, 2006, 17, 457-480.
13. Y. Chen and J. Chen, *Applied Surface Science*, 2016, 387, 16-27.
14. Y. Liu, J. Zhao, Y. He, J. Feng, T. Wu and D. Li, *Journal of Catalysis*, 2017, 348, 135-145.

This journal is © The Royal Society of Chemistry 20xx

15. Y. N. Liu, J. T. Feng, Y. F. He, J. H. Sun and D. Q. Li, *Catalysis Science & Technology*, 2015, 5, 1231-1240.
16. A. J. McCue, A. Guerrero-Ruiz, C. Ramirez-Barria, I. Rodríguez-Ramos and J. A. Anderson, *Journal of Catalysis*, 2017, 355, 40-52.
17. G. X. Pei, X. Y. Liu, A. Wang, A. F. Lee, M. A. Isaacs, L. Li, X. Pan, X. Yang, X. Wang, Z. Tai, K. Wilson and T. Zhang, *ACS Catalysis*, 2015, 5, 3717-3725.
18. G. X. Pei, X. Y. Liu, X. Yang, L. Zhang, A. Wang, L. Li, H. Wang, X. Wang and T. Zhang, *ACS Catalysis*, 2017, 7, 1491-1500.
19. S. Zhang, C.-Y. Chen, B. W. L. Jang and A.-M. Zhu, *Catalysis Today*, 2015, 256, 161-169.
20. H. Zhou, X. Yang, L. Li, X. Liu, Y. Huang, X. Pan, A. Wang, J. Li and T. Zhang, *ACS Catalysis*, 2016, 6, 1054-1061.
21. H. B. Vasili, B. Casals, R. Cichelero, F. Macià, J. Geshev, P. Gargiani, M. Valvidares, J. Herrero-Martin, E. Pellegrin, J. Fontcuberta and G. Herranz, *Physical Review B*, 2017, 96, 014433.
22. D. He, D. Chen, H. Hao, J. Yu, J. Liu, J. Lu, F. Liu, G. Wan, S. He and Y. Luo, *Applied Surface Science*, 2016, 390, 959-967.
23. X. I. Pereira-Hernández, A. DeLaRiva, V. Muravev, D. Kunwar, H. Xiong, B. Sudduth, M. Engelhard, L. Kovarik, E. J. M. Hensen, Y. Wang and A. K. Datye, *Nature Communications*, 2019, 10, 1358.
24. T. W. van Deelen, C. Hernández Mejía and K. P. de Jong, *Nature Catalysis*, 2019, 2, 955-970.
25. M. Kottwitz, Y. Li, R. M. Palomino, Z. Liu, G. Wang, Q. Wu, J. Huang, J. Timoshenko, S. D. Senanayake, M. Balasubramanian, D. Lu, R. G. Nuzzo and A. I. Frenkel, *ACS Catalysis*, 2019, 9, 8738-8748.
26. J. H. Kang, E. W. Shin, W. J. Kim, J. D. Park and S. H. Moon, *Journal of Catalysis*, 2002, 208, 310-320.
27. J. Resasco, L. DeRita, S. Dai, J. P. Chada, M. Xu, X. Yan, J. Finzel, S. Hanukovich, A. S. Hoffman, G. W. Graham, S. R. Bare, X. Pan and P. Christopher, *Journal of the American Chemical Society*, 2020, 142, 169-184.
28. C.-T. Kuo, Y. Lu, L. Kovarik, M. Engelhard and A. M. Karim, *ACS Catalysis*, 2019, 9, 11030-11041.
29. L. Xu, E. E. Stangland and M. Mavrikakis, *Journal of Catalysis*, 2018, 362, 18-24.
30. Y. Zhang, W. Diao, J. R. Monnier and C. T. Williams, *Catalysis Science & Technology*, 2015, 5, 4123-4132.
31. Y. Zhang, W. Diao, C. T. Williams and J. R. Monnier, *Applied Catalysis A: General*, 2014, 469, 419-426.
32. A. Zecchina, E. Groppo and S. Bordiga, *Chemistry – A European Journal*, 2007, 13, 2440-2460.